

MODIFICATION OF SEPIOLITE BY TREATMENT WITH FLUORIDES: STRUCTURAL AND TEXTURAL CHANGES

MARÍA JESÚS BELZUNCE,¹† SAGRARIO MENDIOROZ¹ AND JERZY HABER²

¹ Instituto de Catálisis y Petroleoquímica, CSIC, Campus de la UAM, Cantoblanco, 28049 Madrid, Spain

² Institute of Catalysis and Surface Chemistry, Polish Academy of Sciences, ul. Niezapominajek, 30239 Kraków, Poland

Abstract—In the search for new applications of natural silicates, various F⁻ treatments have been applied to sepiolite to increase its acidic properties and for use as a catalyst in reactions occurring via carbonium ions. Two types of treatments including hydrofluoric acid (HF) at different concentrations and 2 N NH₄F have been utilized and the physicochemical characteristics of the resulting materials studied using standard techniques. The X-ray diffractogram (XRD) patterns indicate a decrease in crystallinity of the original material as well as the appearance of amorphous silica. SEM micrographs showed a shortening and aggregation of the sepiolitic fibers. X-ray photoelectron spectroscopy (XPS), Fourier transform infrared (FTIR), thermogravimetric analysis/differential thermal analysis (TGA/DTA), N₂ adsorption-desorption isotherms and Hg intrusion were used to study the changes occurring in the structure, surface area and pore distribution of samples and acidity was evaluated by IR and thermoprogrammed desorption (TPD) of adsorbed ammonia and pyridine. It was found that acidity increased in most of the samples after anionic and cationic interchange between the activating agents and the surface sites, or extralattice cations. Additionally, structural changes induced by treatments modified the Brönsted and Lewis acidity. Mild treatments with ammonium fluoride are more effective than HF treatments in acidity generation.

Key Words—Activation, Fluoride Activation, Sepiolite, Silicate Acidity.

INTRODUCTION

Clay minerals have many applications related to adsorption and catalysis; in particular, the latter makes use of the acidic-basic properties of the clay mineral surface, as well as the morphology of the mineral to catalyze carbonium ion reactions.

Sepiolite is among the less-studied clays in the context of catalysis, but its large surface area, crystalline structure, porosity and surface acidity may lead to a wide range of applications, especially if activation treatment is able to increase the number and strength of its surface acidic sites. These observations suggest that the mineral deserves more thorough and detailed study, particularly with regard to its modification and potential for application in carbonium ion reactions.

The structure of sepiolite generates permanent microporosity, 10.6 by 3.7 Å in cross-sectional area, and also leads to a fiberlike morphology with an open structure made up of cylindrical pores. Mean fiber length, depending on the deposit, ranges between 0.2 and 2 μm in size. Surface area, which may reach 800 m² g⁻¹, also depends on the deposit and the history of the mineral, but generally ranges between 120–350 m² g⁻¹. Sepiolite is a cheap, very abundant material currently used as an adsorbent and catalyst or catalyst support, its surface reactivity stemming from surface sites of various types (Theng 1974; Serratos 1979; Ruiz-Hitzky and Casal 1985; Campelo et al. 1989).

There are many publications which describe the modification of sepiolite by acid treatment, using H₂SO₄ (Campelo et al. 1989), HNO₃ (López-González et al. 1981) or HCl (Abdul-Latif and Weaver 1969; Fernández Alvarez 1972; González et al. 1984; Corma et al. 1986). Depending on the duration and intensity of the treatment, the reported results of the acid attack are protonization of exchangeable cations and edge Mg²⁺, followed by dissolution of the brucitic octahedral sheet with release of Mg²⁺ cations and creation of silanol groups from the broken surface siloxane groups (Barrios-Neira et al. 1974). With stronger treatment, the presence of free silica has been reported (Fernández Alvarez 1972).

As far as we know, no study has been reported in which HF is used as the activating agent for sepiolite. In contrast, the insertion of F⁻ into the montmorillonite structure has been widely studied. Several authors have reported on the changes in structure and catalytic properties of montmorillonite after activation by solutions of HF, KF, NH₄F (Brückman et al. 1976) and NH₄HF₂ (Fijał et al. 1985). In general, these investigators observed that activation results in an increase in the number of acid centers and, consequently, the application of the material to acid catalysis is facilitated. The changes caused by fluorination are also accompanied by an increase in surface area and porosity, mainly in the meso- and macropore range. Treatment of sepiolite with F⁻ could likewise result in changes in the texture and the number and strength of the surface acidic sites after substitution, through anionic exchange, of surface -OH groups by the more electro-

† Present Address: Dpto de Oceanografía y Medio Ambiente Marino (AZTI), Sarrástegi 8, 20008 San Sebastian, Spain.

negative anion F^- (Gerberich et al. 1966; O'Reily 1966; Matulewicz et al. 1980; Barthomeuf 1985) and subsequent protonization of vicinal OH^- s. Ammonium fluoride has also been used to introduce additional acidity to various samples (Matulewicz et al. 1980, Urabe et al. 1988) by anionic and/or cationic interchange with surface $-OH$ or with the exchangeable cations in the sample, giving rise after thermal treatment to protonic acidity by NH_3 evolution. For this reason, 2 N NH_4F and different concentrations of HF were used in this work as activating agents for sepiolite and their effects on the structure, surface area and pore distribution of the treated material were studied.

EXPERIMENTAL

Material

Material supplied by Tolsa from the Vallecas-Vicálvaro deposit consisting of 95% sepiolite, 263 $m^2 g^{-1}$ surface area and 1.34 $cc g^{-1}$ pore volume, in meso- and macropores, was used for this work. Prior to its use, the secondary minerals (5%), primarily detrital quartz, were separated from the original material. The particle size used in this experiment ranged from 0.20 to 0.32 mm.

Activation Treatment

The activation of sepiolite was accomplished using the following procedure:

1) Hydrofluoric acid solutions at concentrations of 0.1, 0.5 and 1 N were prepared and kept in contact with the sepiolite sample in a 1:100 solid/liquid ratio at room temperature for 1 h. The treated samples were washed with distilled water, dried at 105 °C and stored in a desiccator. Three modified sepiolites were obtained, hereafter identified as SF01, SF05 and SF1, respectively.

2) Sepiolite was added to 2 N NH_4F solutions in a 1:100 solid/liquid ratio and maintained at a temperature of 60 °C for treatment times of 1, 5 and 10 h, respectively, with continuous stirring. The samples were subsequently washed with distilled water, dried at 105 °C and stored in a desiccator. The resulting modified samples were labeled SN1, SN5 and SN10, respectively.

3) After careful characterization, the most promising samples were subjected to thermal treatment at 550 °C for 2 h.

Experimental Techniques

An ISI DS-130 scanning electron microscope (SEM) was used to perform the morphological study of the samples. Coupled to it was an Si/Li detector and a Kevex 8000-II processor with a Be window of 7 μm thickness for energy dispersive X-ray (EDX) analysis of the elements with an atomic number higher than that of Na. The accelerating voltage was 20 keV.

The samples, prior to morphological and chemical analysis, were coated by sputtering in a Polaron E 500 unit with vaporized Au and C, respectively. The XRD patterns were recorded by a DRON-2 diffractometer using $CuK\alpha$ radiation with $\lambda = 1.5418 \text{ \AA}$ and a Ni filter.

Thermal analyses (TGA and DTA) were performed using Perkin-Elmer equipment consisting of a TGS-2 microbalance, a DTA 1700 differential thermal analyzer, a temperature controller system 7/4 and a DS-3600 data station. The heating rate was maintained at 10 °C min^{-1} in a flowing air atmosphere of 80 $cc min^{-1}$.

The apparatus used for study and identification of surface groups before and after exposure to ammonia and pyridine was a NICOLET FTIR spectrometer model 5ZDX. The evolution of acidity with temperature on previously treated samples, 1 h at 400 °C (ammonia) and 200 °C (pyridine), respectively, was studied at room temperature after 1 h stepwise heating of the samples at 25, 100, 170, 270, and 450 °C, respectively.

A Leybold-Heraeus LHS-10 spectrometer equipped with a Mg source ($MgK\alpha = 1253.6 \text{ eV}$) operating at 12 kV and 10 mA, was used for analysis of the chemical state of the surface through XPS. The residual pressure within the analysis chamber was less than $1 \cdot 10^{-8}$ torr; the C_{1s} peak at 284.6 eV was taken as reference for determination of the binding energies.

The surface area and pore size distribution of the samples was determined in 2 ways: 1) N_2 adsorption-desorption at $-197 \text{ }^\circ C$ on previously degassed samples at RT and 10^{-4} torr pressure for BET surface area and meso-micropore distribution, and 2) Hg intrusion for macropore analysis. The equipment consisted of ASAP 2000 and a Poresizer 9310, both from Micromeritics. The pore size distribution of the samples was calculated in accordance with the BJH method (Barrett et al. 1951) for N_2 adsorption-desorption data and the Washburn equation (Washburn 1921) for Hg intrusion data.

Residual acidity was estimated through ammonia adsorption using a conventional glass apparatus. The samples previously treated at 400 °C for 1 h were submitted to 48–50 torr of NH_3 for 15 min at RT. Subsequent thermoprogrammed desorption (TPD) experiments were carried out by heating at 10 °C min^{-1} in the 25–450 °C range.

RESULTS

Chemical and Mineralogical Composition

The results of the chemical analyses made by EDX are summarized in Table 1. In spite of the limitations of the technique, it can be deduced that the chemical treatment caused a progressive dissolution of the octahedral sheet of sepiolite with release of Mg^{2+} , and

Table 1. EDX analysis† of natural (S) and treated samples (SF and SN series).

Sample	MgO	SiO ₂	K ₂ O	CaO	Fe ₂ O ₃	SiO ₂ /MgO
S	30.0	67.5	0.6	1.4	0.4	2.25
SF01	23.7	70.9	1.8	2.4	1.3	2.99
SF05	17.0	79.2	0.6	2.2	2.2	4.65
SF1	26.7	71.1	0.8	1.0	—	2.66
SN1	29.1	66.3	0.4	3.3	0.9	2.27
SN5	27.2	69.9	—	2.9	—	2.57
SN10	26.3	71.8	—	1.9	—	2.73

† The values obtained for MgO and SiO₂ were corrected according to the theoretical composition of sepiolite, Si₁₂Mg₈(OH)₄(H₂O)₄·8H₂O.

corresponding increase in the SiO₂/MgO ratio of the treated samples. The SN1 sample is an exception to this trend.

Figure 1 shows the X-ray diffractograms of the natural and modified samples. The starting material consists primarily of pure sepiolite; only the 3.04-Å reflection may be assigned to calcite present as accompanying material. The modified samples display the characteristic sepiolite reflections indicating that the sepiolite structure persists after the treatment. In the SN series, a broadening of the characteristic sepiolite peaks, as well as a decrease in their intensities, indicate a decrease in crystallinity with respect to the original sample. However, there is no clear indication that this loss of crystallinity increases with extension of the treatment. With respect to the SF samples, an amorphous component is indicated by wide band between 10 and 18 °2θ and this is attributed to amorphous silica. After heating at 550 °C, the SF samples lost the most intense sepiolite reflection *d*(110), which persists in the SN5 and SN10 samples after heating.

Morphology

The modified samples were examined by SEM and representative micrographs are shown in Figure 2. Although the fibrous morphology of the particles was preserved, a more randomly oriented structure resulting from breaking of the fiber bundles is observed in both HF- and NH₄F-treated samples. A distinctive breaking of the primary particles, further aggregation to form thicker bundles, can also be seen in the SN1 and SF05 micrographs. Apparently, the shortening and aggregation of the fibers increases with the strength of the acid. An average length of 2 μm was calculated for natural sepiolite fibers and this value decreases to about 1 μm in the SF05 and SF1 samples. Fiber bundles have widths ranging from 150 to 750 nm from SF01, from 150 to 400 nm for SF05 and from 200 to 990 nm for SF1. Thus, the length/width ratio of the fibers in the treated samples is less than that of the original material. Finally, thermal treatment causes a general disorder of the fibers by separating and apparently shortening them (SF05-500 micrograph).

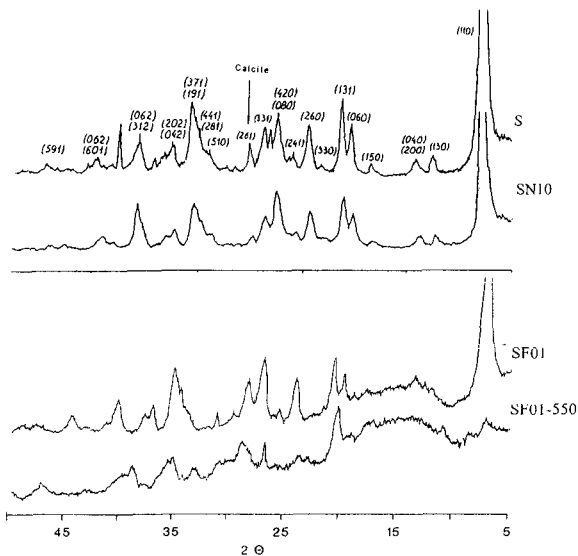


Figure 1. XRD patterns of natural (S) and treated samples (SN and SF series).

Thermal Properties

Table 2 summarizes the temperature intervals and the weight losses corresponding to the different dehydration and dehydroxylation stages for each of the samples. A displacement of the DTG peaks to lower temperatures is observed for zeolitic and coordinated water in the SF samples as well as a general decrease in peak intensity for the activated samples with respect to the original material (Figure 3). The DTA patterns show that the low-temperature endothermic peak, corresponding in sepiolite to physisorbed and zeolitic water, is more intense than in the treated samples. Also, the second and third endothermic peaks decrease in intensity in the treated samples compared to the original material. Finally, the endo-exothermic peak characteristic of sepiolite at around 800 °C is less visible in the treated samples, and almost disappears in the SN series.

Surface Area and Pore Size Analysis

Representative N₂ adsorption-desorption isotherms are shown in Figure 4. The isotherms are type IV according to the BDDT classification and exhibit a H₁ + H₃ type of hysteresis loop corresponding to slit-shaped porosity among particles with inner open cylindrical pores (Sing et al. 1985). Apparently, the activated sepiolite maintains its acicular morphology during the treatments. The absence of saturation at high relative pressures reveals the presence of macropores.

The results in Table 3a show that treatment with HF does not result in as large a variation in the sample surface area and total pore volume as treatment with NH₄F. As micro- and mesoporosity do not change appreciably after treatments of both types of samples, the

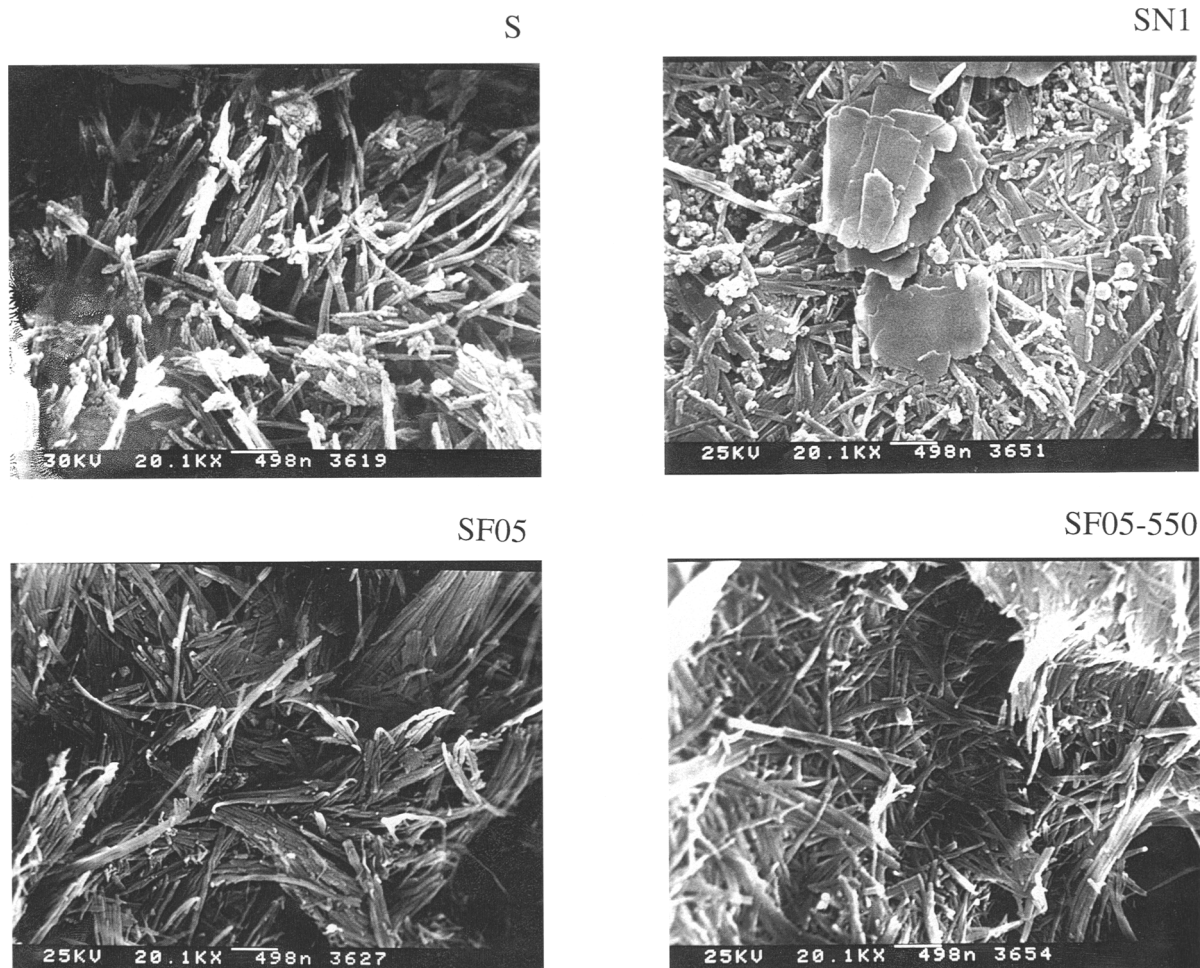


Figure 2. Scanning electron micrographs of natural (S) and treated samples (SN1, SF05 and SF05-500).

Table 2. Water loss through thermogravimetric analysis of natural (S) and treated samples (SF and SN series).

		Steps of dehydration†					Total loss
		I	II	III	IV	New phase	
S	T(°C)range	<240	240–445	445–610	610–780	780–950	19.20
	wt loss %	12.70	3.80	2.50	1.70	1.90	
SF01	T(°C)range	<240	240–425	425–620	620–770	770–935	20.00
	wt loss %	11.00	3.40	3.08	0.80	1.72	
SF05	T(°C)range	<220	220–430	430–630	630–775	775–925	19.20
	wt loss %	10.68	3.32	2.60	1.00	1.60	
SF1	T(°C)range	<220	220–430	420–630	630–775	775–940	19.60
	wt loss %	11.20	3.32	2.68	0.72	1.68	
SN1	T(°C)range	<240	240–425	425–625	625–750	750–920	16.30
	wt loss %	8.00	3.40	2.60	1.00	1.32	
SN5	T(°C)range	<250	250–430	430–630	630–750	750–915	18.60
	wt loss %	11.20	3.00	2.52	0.68	1.20	
SN10	T(°C)range	<250	250–430	420–630	630–775	775–940	16.30
	wt loss %	9.20	3.12	2.00	0.80	1.20	

† I: zeolitic water, II: 1st coordination water, III: 2nd coordination water, IV: structural water.

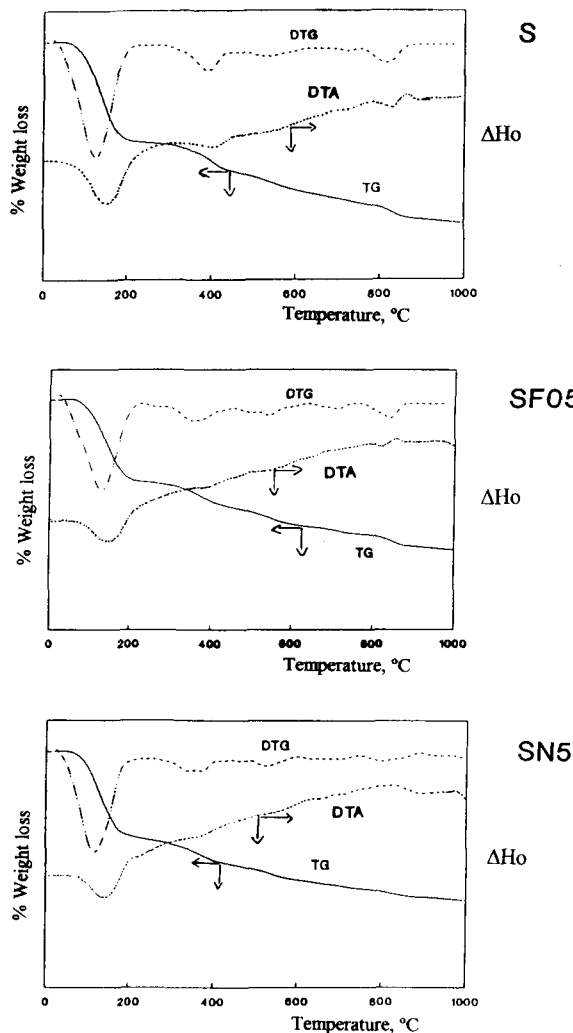


Figure 3. TG, DTG and DTA curves of natural (S) and treated samples (SF05 and SN5).

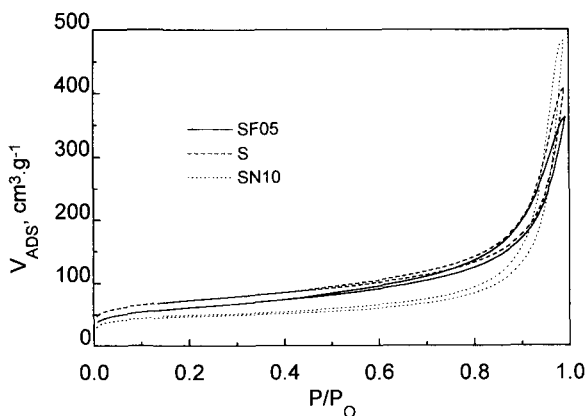


Figure 4. N₂ adsorption-desorption isotherms of natural (S) and treated samples (SN and SF series).

Table 3a. Surface area and pore size distribution of natural (S) and treated (SF and SN series) samples.

Sample	$S_{BET}, m^2 g^{-1}$	$V_{\text{pore}}, cm^3 g^{-1}$			D, nm
		$V_{\mu p}$	V_{mp}	V_{Mp}	
S	263	0.04	0.32	0.98	20.4
SF01	282	0.05	1.31	1.03	19.3
SF05	218	0.03	0.33	0.97	24.4
SF1	249	0.06	0.40	1.25	27.3
SN1	298	0.02	0.32	1.00	27.0
SN5	238	0.05	0.29	0.64	16.5
SN10	176	0.04	0.30	0.37	16.1

reduction in pore volume found for SN samples may be attributed to changes in macropores. These changes can be detected by Hg intrusion data, an example of which is given in Figure 5. There is a trimodal distribution of pores in all samples, whose frequency varies with the treatment. The maximum in pore volume arises mainly from pores in the 6–200 μm size range in all samples, increasing with the intensity of the treatments, except the final SF1 and SN10 treatments. Since this part of the poregram is usually ascribed to interparticulate voids, an effective increase in the corresponding particle size, perhaps by destruction and reaggregation of the fibers as suggested by SEM, may be indicated. In contrast, pores in the 0.4 to 6 μm size range decrease, while those in the 0.06 to 0.4 μm range increase slightly with the treatments. All samples exhibited a sharp reduction in surface area after thermal treatment, up to 50% compared to that of the parent material (see Table 3b). An increase in the amount of large pores was also observed in the samples following thermal treatment.

Structure

The character of surface groups of the samples was studied by IR and XPS. IR spectra (Figure 6) show that the treated material generally retained the characteristic spectrum of the original sepiolite with some variations in the intensity and wavenumber of the bands: thus, there is a reduction in the intensity of the

Table 3b. Surface area and pore size distribution of natural (S) and treated (SF and SN series) samples after 550 °C 2 h.

Sample	$S_{BET}, m^2 g^{-1}$	$V_{\text{pore}}, cm^3 g^{-1}$			D, nm
		$V_{\mu p}$	V_{mp}	V_{Mp}	
S	140	0.010	0.31	1.01	38.0
SF01	110	0.002	0.31	1.15	53.1
SF05	121	0.004	0.30	1.15	48.0
SF1	168	—	0.34	2.18	60.0
SN1	128	0.007	0.32	1.46	55.6
SN5	112	0.004	0.28	1.46	62.1
SN10	102	0.022	0.24	0.76	40.0

S_{BET} : BET surface area, $V_{\mu p}$: volume of micropores, V_{Mp} : volume of macropores, V_{mp} : volume of mesopores, D : pore diameter.

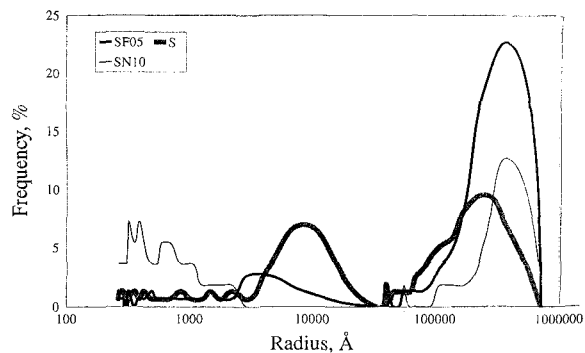


Figure 5. Macropore distribution of natural (S) and treated samples (SF05 and SN5).

bands corresponding to zeolitic water in the stretching ($\sim 3400\text{ cm}^{-1}$) and bending ($\sim 1659\text{ cm}^{-1}$) regions; and the band at 1695 cm^{-1} corresponding to coordinated water disappears in the SF1, SN5 and SN10 samples. The bands at 3680 cm^{-1} and 648 cm^{-1} , assigned to the stretching and bending vibrations of structural hydroxyl groups bonded to octahedral Mg, also decrease with treatment, as does the characteristic band for sepiolite at 1210 cm^{-1} . In contrast, the intensity of Si-O bonding vibrations: stretching (1024 cm^{-1}), deformation (1077 and 980 cm^{-1}) and bending (474 cm^{-1}), attributed to silica, become more intense, as the strength of the treatment increases.

Thermal treatment at $550\text{ }^{\circ}\text{C}$ resulted in the disappearance of the characteristic sepiolite 1210-cm^{-1} band, as well as the Si-O deformation bands and the stretching vibration triplet. A broad band appears cen-

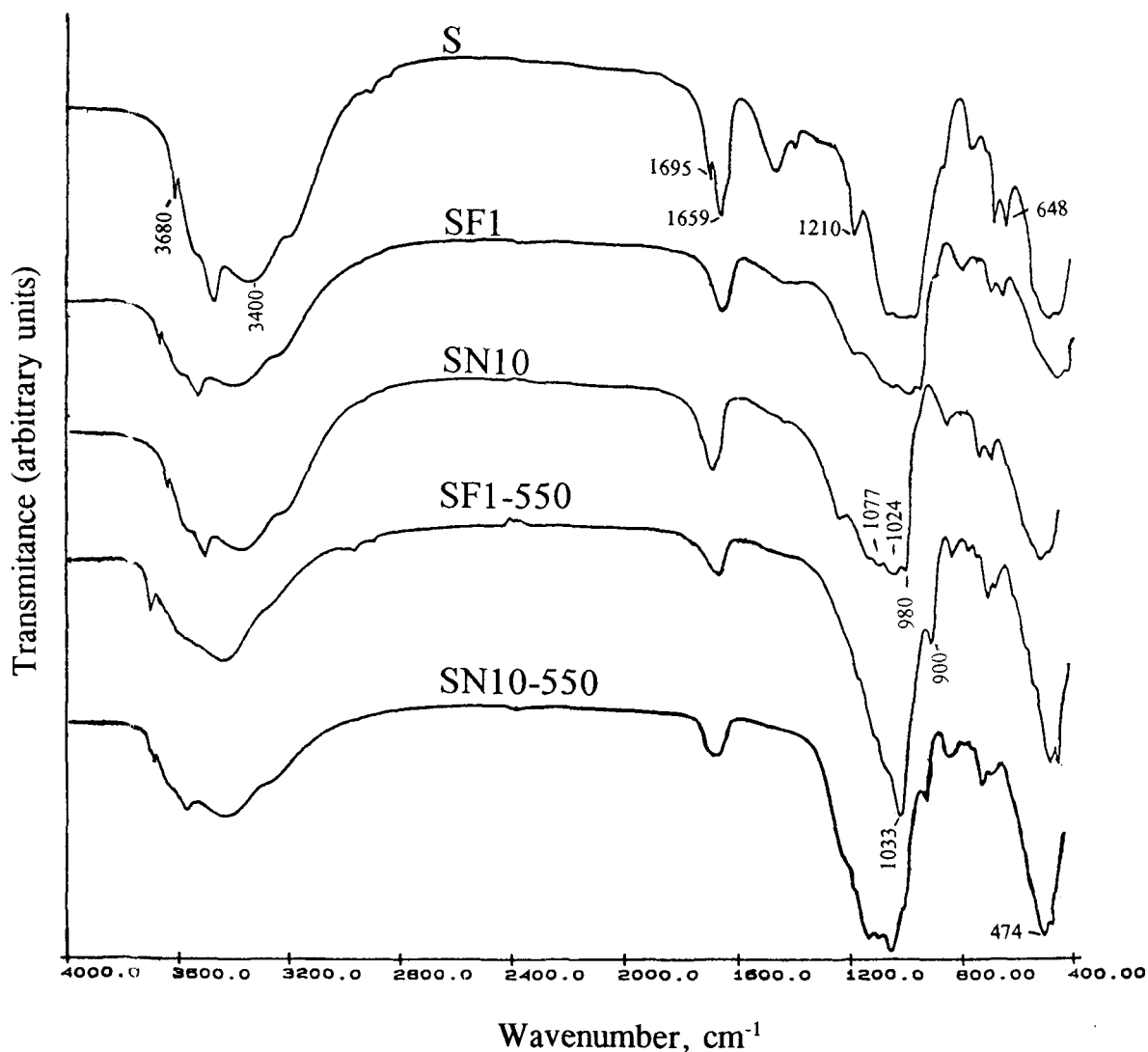


Figure 6. IR spectra of natural (S) and treated samples (SN and SF series).

Table 4a. Bonding Energy (eV) of electrons in internal levels for natural (S) and treated samples (SF and SN series) as determined by XPS.

Sample	Si 2p	Mg 2p	Ca 2p	F 1s	N 1s
S	103.4	nm†	346.9	nm	nm
SF01	103.4	nm	nm	686.1	nm
SF05	103.4	50.8	349.7	686.3	nm
SF1	103.4	50.5	349.5	686.4	nm
SN1	103.4	nm	nm	688.9	400.3
SN5	103.4	nm	347.5	684.5	400.8
SN10	103.4	nm	347.3	684.6	401.0

† nm: not measured.

tered at 1033 cm^{-1} , characteristic of amorphous silica, as well as a band at 900 cm^{-1} .

Tables 4a and 4b summarize the results obtained by XPS. There are no variations in the bonding energies of Si and Mg in both fresh and treated samples, which indicates that they maintain their environment throughout the treatment. However, F 1s in the SN series shows a higher BE on SN1 and a lower one on SN5 and SN10 compared to the SF series. Furthermore, the BE of Ca 2p is slightly higher in the SF sample than in the natural and SN samples.

The surface atomic ratios F/Si and N/Si are indicative of the incorporation of F^- and NH_4^+ ions into the mineral structure, probably by ionic substitution of the most superficial OH^- groups by F^- and of the octahedral or exchangeable cations by NH_4^+ (Table 4b).

Acidity

The acidity of the samples was studied by TPD of ammonia. Table 5 shows the amount of adsorbed ammonia after 15 min exposure. A sharp increase in the number of acid sites per square meter on samples SF01 and SN1 is visible, whereas samples SF1 and SN5 remain unaffected, and samples SF05 and SN10 have an intermediate position.

The TPD curves (Figure 7) show at least 3 types of acid centers corresponding to desorption at 100, 170 and 270 $^\circ\text{C}$, respectively. The number and acid strength of these centers varies with the applied treatment, those at 100 and 170 $^\circ\text{C}$ being very weak. A fourth type is also seen in samples SF01, SF1, SN1

Table 4b. Surface atomic ratios for natural (S) and treated samples (SF and SN series) as determined by XPS.

Sample	F/Si	Ca/Si	N/Si	F/N
S	—	0.0095	nm	nm
SF01	0.093	nm	nm	nm
SF05	0.058	0.0049	nm	nm
SF1	0.085	0.0065	nm	nm
SN1	0.043	nm	0.0370	1.16
SN5	0.317	nm	0.0093	34
SN10	0.164	nm	0.0090	18

† nm: not measured.

Table 5. Adsorbed ammonia by natural (S) and treated samples (SF and SN series) after degassing.

Sample	NH_3 adsorbed $\mu\text{mol g}^{-1}$	Acid sites $\text{m}^{-2} \times 10^{18}$
S	263	1.14
SF01	320	1.74
SF05	240	1.20
SF1	281	1.00
SN1	350	1.64
SN5	190	1.02
SN10	201	1.19

and SN10, associated with a broad peak around 410 $^\circ\text{C}$, although it is difficult to be certain.

Figure 8 shows, at each temperature, the normalized number of acid centers (taken as peak height) in the activated samples with respect to natural sepiolite. From this representation it may be deduced that both treatments increase the number of weak acid centers and decrease the number of mild-strong ones in all samples, except sample SN1. As a consequence, only the milder treatments, with 0.1 HF and 1 h 2 N NH_4F , provide the samples with the intended increase in strong acidity.

The nature of acid centers (Brønsted-Lewis) present in the SF samples as well as the changes produced therein as a result of the treatment, were studied by IR spectroscopy of adsorbed ammonia: 2 new peaks appeared in their spectra at 3295 cm^{-1} corresponding to NH_4^+ bonded to Brønsted centers and 3375 cm^{-1} corresponding to NH_3 bonded to Lewis centers. Under thermal treatment, all samples, except SF05, retained

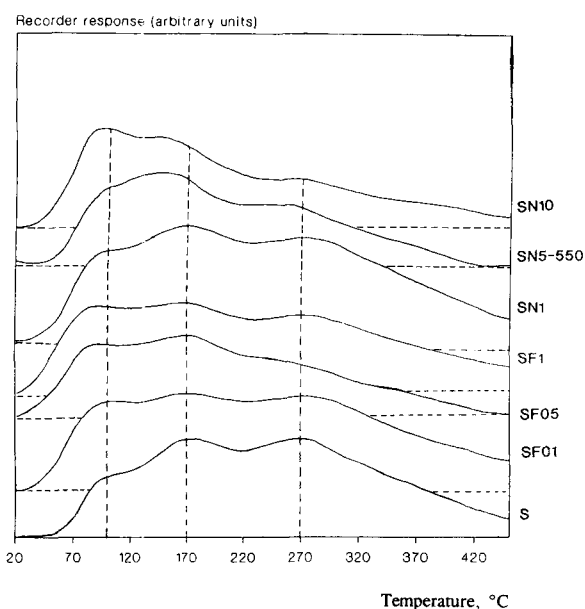


Figure 7. Ammonia TPD curves of natural (S) and treated samples (SF series).

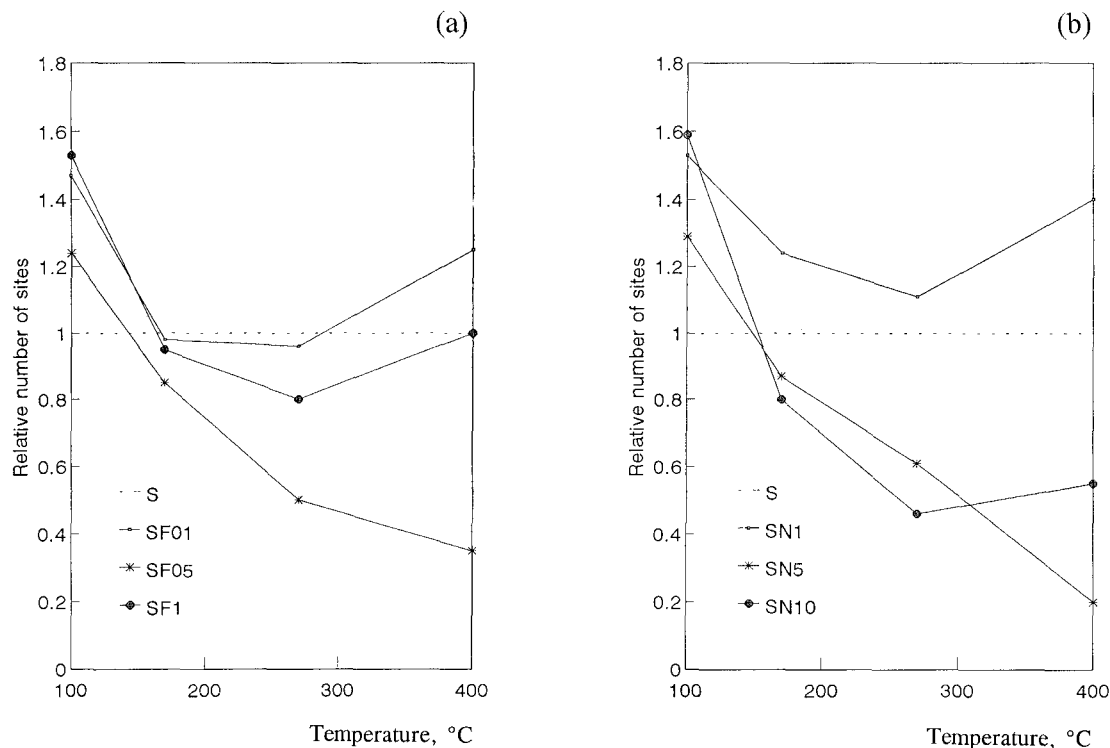


Figure 8. Distribution of acidity on activated samples with respect to natural sepiolite (from TPD experiments): a) SF; b) SN samples.

the band at 3375 cm^{-1} up to $450\text{ }^{\circ}\text{C}$, whereas that at 3295 cm^{-1} disappeared at $170\text{ }^{\circ}\text{C}$ on SF05, at $270\text{ }^{\circ}\text{C}$ on SF1 and was retained up to $450\text{ }^{\circ}\text{C}$ in the SF01 sample. These findings point to the presence of strong acid sites of both Brönsted and Lewis type on SF01 and, to a lesser extent, on SF05 and SF1 samples.

After RT adsorption of pyridine, the resulting IR spectra of SN samples (Figure 9) revealed the appearance of bands at 1613 , 1574 and 1443.8 cm^{-1} , characteristic of pyridine adsorbed on Lewis centers: a weak band at 1545 and a shoulder at 1590 cm^{-1} which appear to be unstable above $100\text{ }^{\circ}\text{C}$, due to the adsorption of pyridine on Brönsted acid sites. Bands at 1393 and 1490.9 cm^{-1} reflect both Lewis and Brönsted acidity. Thus, both types of acidity are present on the samples, remaining more or less unchanged up to $450\text{ }^{\circ}\text{C}$.

DISCUSSION

The results of these experiments show that chemical treatment causes a partial dissolution of the octahedral sheet with release of octahedral Mg^{2+} and amorphous silica formation. This has been observed previously in sepiolite treated with other acids and it also occurs in montmorillonite (Mendioroz et al. 1987) and palygorskite (Gonzalez et al. 1989). The resulting free silica ultimately polymerizes, depending on the pH of the

solution and the saline effect of the previously extracted cations (from the octahedral sheet as well as from the impurities accompanying the sample), and is deposited on the sample, coating it and eventually impeding further attack. In the treated samples, the SiO_2/MgO ratio follows the sequence:



from which it can be inferred that the above-mentioned effect is more pronounced on acid-treated samples than on those treated with ammonium fluoride. However, quantifying the proportion of Mg and Si in the activated samples is problematical because chemical analyses were made by EDX. This means that the layer analyzed was no more than $2\text{ }\mu\text{m}$ thick, and as the intensity of the Mg peak was very weak, the data shown in Table 1 may be relative rather than absolute values. Nevertheless, the results are consistent with those obtained by XRD showing evidence of a clear amorphization of the structure in the SF series, whereas sepiolite in the SN series is almost unaltered.

The amorphization is attributed to the presence of amorphous silica, generated as a consequence of the partial leaching of the octahedral sheet and subsequent reorganization of the tetrahedra of the original material. With progressive acid attack, the crystallinity of the samples decreased, as can be seen from the de-

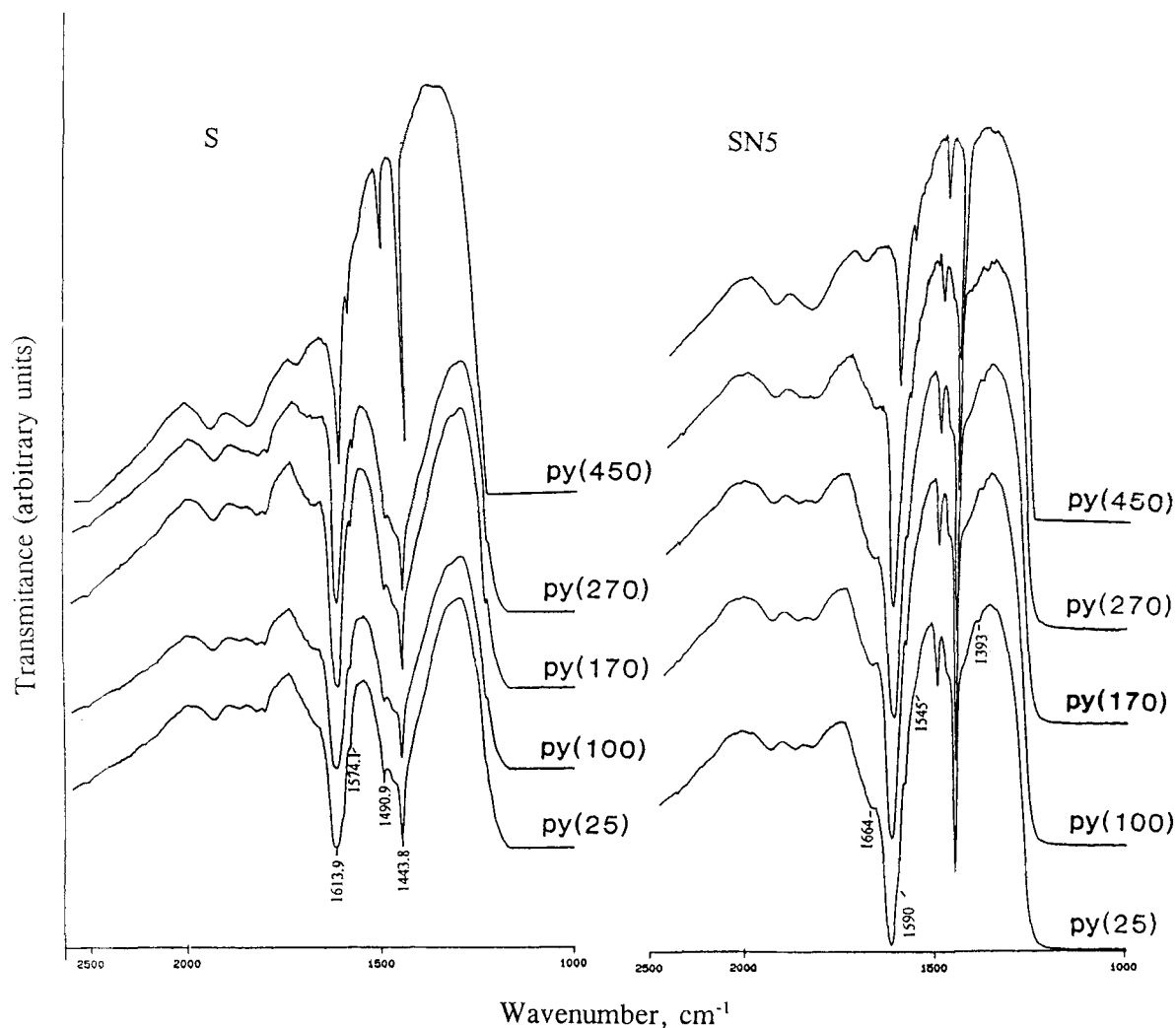


Figure 9. IR spectra of adsorbed pyridine on S and SN5 samples (temperature range 25 to 450 °C).

crease in intensity of the characteristic XRD peaks. Free silica may contribute to the reaggregation of the fibers indicated in the SEM micrographs. Thermal treatment results in folding and disaggregation of the fibers caused by dehydration around 350 °C, and loss of coordinated water from both sepiolite and agglutinating amorphous silica.

The presence of amorphous silica in the activated samples is also supported by the smaller weight losses with respect to natural sepiolite, recorded by TGA in the 240–425 °C range corresponding to the reduced amounts of crystallization water. The changes shown in the IR spectra (Figure 6) are again consistent with the formation of amorphous silica and show a reduction of the bands attributed to sepiolite and the increase in those corresponding to Si-O bond vibrations.

The appearance in the DTG curves of the SN series of a new peak at a lower temperature may be attributed

to the partial substitution of edge Mg^{2+} ions by NH_4^+ and subsequent ammonia evolution during progressive heating. This partial disappearance of Mg^{2+} ions is corroborated by the loss in intensity of the exotherm component in the endo-exothermic peak around 800 °C in DTA. With respect to the SF samples, the peak appearing in the DTG curves in the 430–630 °C range must be ascribed to additional water loss caused by migrating protons inside the clay structure with subsequent interaction with -OH groups within the octahedral sheet (Fripiat 1988).

The surface area and pore size distribution of the samples after activation should represent a combination of features corresponding to un- or partially attacked sepiolite and to amorphous silica resulting from the treatment. No significant difference is shown, however, with respect to the original material in the N_2 adsorption isotherms and the type of hysteresis loop

involved, suggesting that the silica resulting from the treatment preserves the original texture of the sample. In contrast, surface area shows a significant decay in the SN series which may be related to the clogging of the mouths of the meso- and micropores by the generated silica. When the activated samples are submitted to thermal treatment, there are important changes in surface area. It is known that natural sepiolite undergoes "crystal folding" above 350 °C (Preisinger 1963; Nagata et al. 1974; Prost 1976; Serna et al. 1976; Serna and Van Scoyoc 1978; Folgado 1983), reducing surface area to half its original value. A similar behavior might be anticipated from the treated samples if sepiolite remained unaltered, but the loss in surface area of the activated samples induced by heating (Table 3) is much lower than expected. This is consistent with the presence of a component other than sepiolite as a consequence of the transformation brought about by the activation treatment. It is suggested that amorphous silica may act as a cement between the sepiolite fibers inhibiting their folding at a microscopic level and generating larger pores as a consequence of fiber disaggregation.

XPS reveals the presence of F^- and NH_4^+ arising from ionic substitution on the surface of all samples. The degree of substitution differs according to the treatment and is more pronounced during the earlier stages of the attack. In general, NH_4F treatments are much more effective in incorporating F, probably because the acid completely dissolves part of the sepiolite which is washed out after the activation treatment. In contrast, the action of NH_4^+ is merely of ionic interchange, the degree of degradation of the sample being very low. The reported F/N ratios in SN samples indicate that NH_4^+ incorporation is much less effective than F^- incorporation, except for the SN1 sample where the F/N ratio is around 1. This probably results from a larger number of available OH^- than Mg^{2+} ions in sepiolite (or free silica) once the degradation and dissolution of the octahedral sheet has begun after the first stage of the treatment. In addition, the high vacuum (10^{-8} torr) to which the samples are subjected, prior to their analysis by XPS, can result in ammonia evolution from the NH_4^+ ions incorporated on the surface, giving values for surface N smaller than the actual ones. The high value of the BE for F 1s is on SN1 denotes the strong ionic character of the Si-F bond revealing the substitution of F^- by OH^- . Moreover, the technique revealed the presence of Ca^{2+} ions on all samples, with higher bonding energies on SF than on natural and ammonium-treated samples. This is ascribed to the precipitation of CaF_2 or insoluble mixed fluorides (Brückman et al. 1976) after dissolution of calcite by HF.

With regard to acidity, the number of acid sites per square meter increases with treatment in all samples, except for sample SN5, but the acid strength barely

changes (Figure 8). It has long been known that sepiolite has negligible acidity ($H_0 \geq +4$) (Rich 1960; Dandy and Nadiye-Tabbiruka 1982; Rey-Bueno et al. 1985; Villafranca-Sánchez et al. 1987), mostly of the Lewis type, associated with exchangeable cations and surface defects (Campelo et al. 1989; Corma and Pérez-Pariante 1987). It is thought that the breaking of the fibers after activation treatment results in an increase in the number of weak acid sites.

There are 3 sources from which protonic acidity can be created in the activated samples. The first is connected with the asymmetry of the water molecules coordinated to exchangeable or edge cations (Farmer and Mortland 1966; Serna et al. 1976; Serna and Van Scoyoc 1978). When the sepiolite samples undergo "folding" at temperatures above 350 °C, half the water coordinated to the edge cation of the octahedral sheet is lost and the remaining water is easily protonized by displacement of a hydrogen towards the oxygen of the Si-O-Si groups of the tetrahedral sheet. After exposure to ammonia or pyridine, the corresponding deformed ion, ammonium or pyridinium, is formed (Blanco et al. 1988). Since all the samples were submitted to thermal treatment at about 400 °C, prior to exposure to ammonia, an increase in the number of mild acid sites by the treatment, should be expected. However, the lower polarizability of water bound to H^+ in H-sepiolite, instead of Mg^{2+} (following the Ze/R² rule), must decrease the number of mild acid sites except for SN1. Once the coordinated water is lost, NH_3 is retained only by exposed cations or surface defects through their Lewis acidity, the effect being smaller as the fluorine content in the sample increases (Corma et al. 1985). Such is the case for samples SN5 and SN10. The second source of protonic acidity involves the evolution of NH_3 from NH_4^+ during thermal treatment with subsequent protonization of the sample giving rise to strong acidity, such as in SN1. The third source involves F^- after fluorination. The acidity of the silanols is very weak, but the presence of vicinal F^- must enhance their acid strength, giving rise to Brønsted acid sites detectable through NH_3 adsorption. These sites are related essentially to the number of silanols susceptible to exchange and they reach a level that varies with the sample and the intensity of the treatment. After fluorination, hydroxyls of strong acidity should be created, which seems to occur on samples SF01 and SN1.

In this study, the expected strong acidity increased only for samples SF01 and SN1. The other activation treatments were much too strong and degradation of sepiolite occurred, especially when the activating agent was HF. The computed high F^- content is due either to its incorporation by the newly formed amorphous silica or to precipitation with the cations present in the solution arising from leaching of sepiolite and/or partial dissolution of the remaining impurities.

CONCLUSIONS

The treatment of sepiolite with fluorine compounds leads to changes in the morphological-structural-textural characteristics as well as in the acid properties of the samples, which are expected to affect their catalytic activity. The nature of the modifications depends on the treating agent and on the duration of the treatment, concentration and temperature. Mild NH_4F treatments are more effective than HF treatments in the generation of acidity. Both treatments cause cationic (H^+ , NH_4^+) as well as anionic (F^-) surface exchange but also a partial dissolution of the octahedral sheet with release of octahedral Mg^{2+} and formation of amorphous silica. These latter effects are less after NH_4F treatment than after HF treatment.

The balance between both effects, ionic substitution and silica phase formation, should be taken into account in explaining the differences in the morphology, structure and texture that determine the distribution and strength of the various acid sites found in the treated samples. Thus, the elimination or creation of Brønsted and Lewis acid centers is related to the structural changes introduced in the original sample by the treatments performed. Strong treatments result in formation of silica covering the unaffected sepiolite structure which prevents the continuation of structural damage. Therefore, the sample properties reflect a combined effect corresponding to un- or partially attacked sepiolite and to amorphous silica. The total acidity of the samples is affected by the amount of amorphous silica formed and as a consequence the number of weak acid sites.

Anionic (F^-) exchange results in an enhancement of the acid strength up to a certain point, but beyond this, further F^- incorporation is not reflected in a corresponding increase in acidity. Cationic (NH_4^+) exchange affects the coordinated water polarizability, thus decreasing the mild Brønsted acidity of all samples. Furthermore, after thermal treatment, a protonization of the samples is produced after NH_3 evolution, which results in an increase in the acid strength of the samples.

Finally, when activating sepiolite with fluorides, only the use of mild treatments (low concentration of acid or short term exposures to ammonium fluoride) is recommended for F^- or NH_4^+ incorporation into the samples.

ACKNOWLEDGMENTS

MJB wishes to acknowledge the support from the Spanish and Polish Governments under agreement between Spanish Research Council and Polish Academy of Sciences. The authors are greatly indebted to R. E. Ferrell, J. T. Klopogge and A. Juges for their valuable suggestions and comments that have materially improved the quality of this work. MJB is especially grateful to M. J. Wilson for his constant help and encouragement.

REFERENCES

- Abdul-Latif N, Weaver ChE. 1969. Kinetics of acid dissolution of palygorskite (attapulgitite) and sepiolite. *Clays Clay Miner* 17:169–178.
- Barrett EP, Joyner LG, Halenda PP. 1951. The determination of pore volume and area distributions in porous substances. I. Computation from Nitrogen isotherms. *J Am Chem Soc* 73:373–380.
- Barthomeuf D. 1985. *Catalysis by acids and bases*. Amsterdam: Elsevier. B. V. 89 p.
- Blanco C, Herrero J, Mendioroz S, Pajares JA. 1988. Infrared studies of surface acidity and reversible folding in palygorskite. *Clays Clay Miner* 36:364–368.
- Brückman K, Fijał J, Haber J, Kłapyta Z, Wiltowski T, Żabiński W. 1976. Influence of different activation methods on the catalytic properties of montmorillonite. *Mineralogia Polonica* 7:5–12.
- Campelo JM, García A, Luna D, Marinas JM. 1989. Textural properties, surface chemistry and catalytic activity in cyclohexene skeletal isomerization of acid treated natural sepiolites. *Mater Chem Phys* 24:51–70.
- Corma A, Fornés V, Ortega E. 1985. The nature of acid sites on fluorinated γ -alumina. *J Catal* 92:284–295.
- Corma A, Mifsud A, Pérez-Pariente J. 1986. Etude de l'attaque acide de la sepiolite: Modification des propriétés texturales. *Clay Miner* 21:69–84.
- Corma A, Pérez-Pariente J. 1987. Catalytic activity of modified silicates: 1. Dehydration of ethanol catalyzed by acidic sepiolite. *Clay Miner* 22:423–433.
- Dandy AJ, Nadiye-Tabbiruka MS. 1982. Surface properties of sepiolite and its catalytic activity for ethanol decomposition. *Clays Clay Miner* 30:347–352.
- Farmer VC, Mortland MM. 1966. An infrared study of the coordination of pyridine and water to exchangeable cations in montmorillonite and saponite. *J Chem Soc (A)*:344–351.
- Fernández Alvarez T. 1972. Activación de la sepiolita con ácido clorhídrico. *Bol Soc Esp Cerám Vidr* 11:6.
- Fijał J, Żyła H, Tokarz M. 1985. Chemical, sorptive and morphological properties of montmorillonite treated with ammonium bifluoride (NH_4HF_2). *Clay Miner* 20:81–92.
- Folgado MA. 1983. Caracterización textural y estructural de una sepiolita natural y activada. [Ms.Sc. thesis]. Madrid, Spain: Univ Complutense de Madrid. 128 p.
- Fripiat JJ. 1988. High resolution solid state NMR study of pillared clays. *Catal Today* 2:281–295.
- Gerberich H, Lutinski FL, Hall WK. 1966. Studies of the hydrogen held by solids. X. Fluorided aluminas as acid catalysts. *J Catal* 6:209.
- González L, Ibarra LM, Rodríguez A, Moya JS, Valle FJ. 1984. Fibrous silica gel obtained from sepiolite by HCl attack. *Clay Miner* 19:93–98.
- González F, Pesquera C, Blanco C, Benito I, Mendioroz S, Pajares JA. 1989. Structural and textural evolution of Al- and Mg- Palygorskites. I Under acid treatment. *Appl Clay Sci* 4:373–388.
- López-González JD, Ramírez-Sáenz A, Rodríguez-Reinoso F, Valenzuela-Calahorra C, Zurita Herrera L. 1981. Activación de una sepiolita con disoluciones diluidas de HNO_3 y posteriores tratamientos térmicos. I. Estudio de la superficie específica. *Clay Miner* 16:103–113.
- Matulewicz ERA, Kerkhof FP, Moulijn JA, Reistma HJ. 1980. Structure and activity of fluorinated alumina. I. Determination of the number of protonic sites by an IR study of adsorbed pyridine. *J Colloid Interface Sci* 77:110–120.
- Mendioroz S, Pajares JA, Benito I, Pesquera C, Gonzalez F, Blanco C. 1987. Texture evolution of montmorillonite under progressive acid treatment. Change from H3 to H2 Type of Hysteresis. *Langmuir* 3:676–681.

- Nagata H, Shimoda S, Toshio S. 1974. On dehydration of bound water of sepiolite. *Clays Clay Miner* 22:285–293.
- O'Reily DE 1966 *Sbornik "Kataliz"*. Moscow: Moscow Ed. Mir. 55 p.
- Preisinger A. 1963. Sepiolite and related compounds: Its stability and application. *Clays Clay Miner* 10:365–371.
- Prost R 1976. Spectre infrarouge de l'eau présente dans l'attapulgitite et la sepiolite. *Bull Grpe Fr Argiles* 25:53–56.
- Rey-Bueno F, Villafranca-Sánchez M, González-Pradas E, López-González JD. 1985. Adsorción de amoníaco, metilamina y etilamina sobre una sepiolita. *An Quim* 81B:18–21.
- Rich AD. 1960. *Industrial minerals and rocks*, 3rd edition. New York: AIME. 62 p.
- Ruíz-Hitzky E, Casal B. 1985. Epoxide rearrangements on mineral and silica-alumina surfaces. *J Catal* 92:291–295.
- Serna C, Van Scoyoc GE. 1978. Infrared study of sepiolite and palygorskite surface. In: Mortland MM, Farmer VC, editors. *Proc Int Clay Conf*; 1978; Oxford, UK. Amsterdam: Elsevier. p 99–109.
- Serna C, Van Scoyoc GE, Ahlrichs JL. 1976. Uncoupled water found in palygorskite. *J Chem Phys* 65:3389–3390.
- Serratos JM. 1979. Surface properties of fibrous clay minerals (palygorskite and sepiolite). In: Mortland MM, Farmer VC, editors. *Proc Int Clay Conf*; 1978; Oxford, UK. Amsterdam: Elsevier. p 99–109.
- Sing KSW, Everett DH, Haul RAW, Moscou L, Pierotti RA, Rouquero IJ, Siemieniewska T. 1985. Reporting physisorption data for gas/solid systems with special reference to determination of surface area and porosity. *Pure Appl Chem* 58:603–919.
- Theng BKG. 1974. *The chemistry of clay-organic reactions*. London: London Hilger. 343 p.
- Urabe K, Sakurai H, Izami Y. 1988. Cation-exchanged synthetic saponite as a "heat-stable" acidic clay catalyst. *J Chem Soc Chem Commun*:1520.
- Villafranca-Sánchez M, Valverde-García A, González-Pradas E, Rey-Bueno F 1987. Estudio del proceso de retención de anilina por una sepiolita. *An Quim* 83B:151–156.
- Washburn EW. 1921. Note on a method of determining the distribution of pore sizes in a porous material. *Proc Natl Acad Sci USA* 7:115–120.

(Received 15 April 1997; accepted 25 February 1998; Ms. 97-037)